Supplementary Information

Solar-Driven Simultaneous Desalination and Power Generation Enabled by Graphene Oxide Nanoribbons Papers

Yang Sun [a], Zongbin Zhao [a, *], Guanyu Zhao [a], Yongzhen Yang [b], Xuguang Liu [b], Luxiang Wang [c], Dianzeng Jia [c], Xuzhen Wang [a] and Jieshan Qiu [a, d, *]

[a] *State Key Laboratory of Fine Chemicals, Liaoning Key Laboratory for Energy Materials and Chemical Engineering,*
School of Chemical Engineering, Dalian University of Technology, Dalian 116024, China.

[b] *Key Lab of Interface Science and Engineering in Advanced Materials, Ministry of Education, Taiyuan University of Technology, Taiyuan 030024, China*

[c] *Key Laboratory of Energy Materials Chemistry, Ministry of Education, Key Laboratory of Advanced Functional Materials, Autonomous Region, Institute of Applied Chemistry, Xinjiang University, Urumqi 830046, China*

[d] *School of Chemical Engineering, Beijing University of Chemical Technology, Beijing 100029, China*

1. Supporting Figures

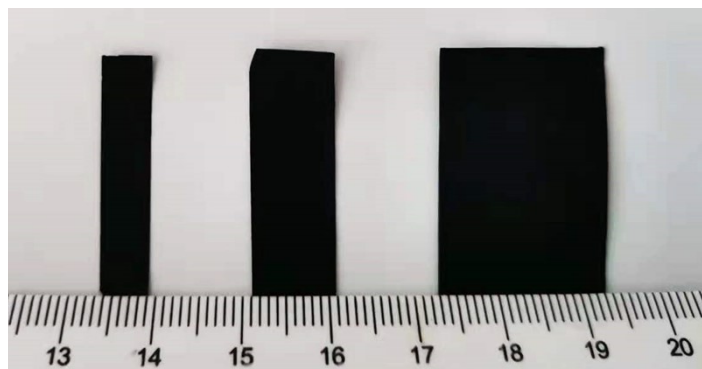* Corresponding authors. E-mail addresses: *zbzhao@dlut.edu.cn (Z. Zhao)*; *jqiu@dlut.edu.cn (J. Qiu)*

Fig. S1 Digital photographs of GONRs-Ba paper with different size: 0.5 cm × 3 cm, 1 cm× 3 cm, and 2 cm × 3 cm, respectively.
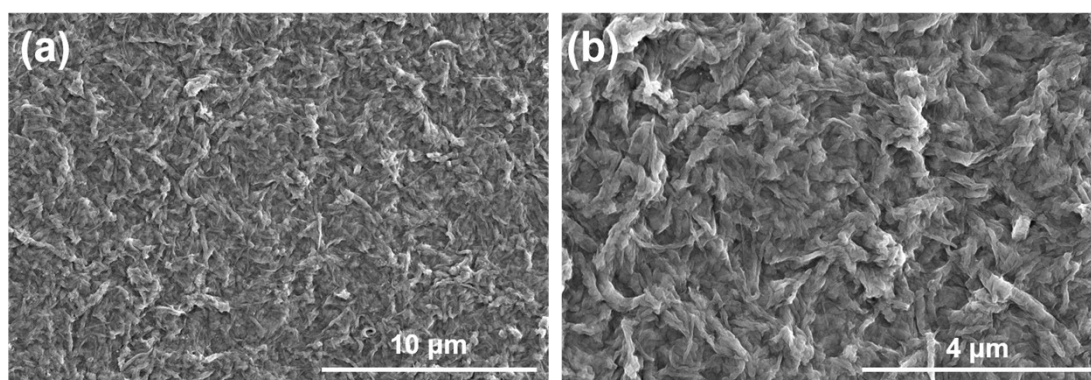

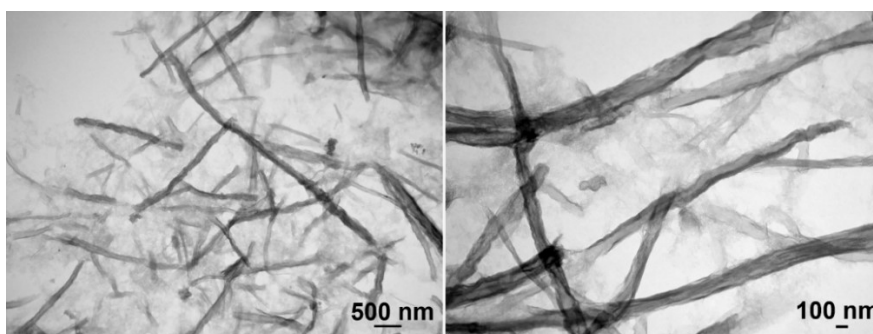**Fig. S2** FESEM images of GONRs-Ba paper.
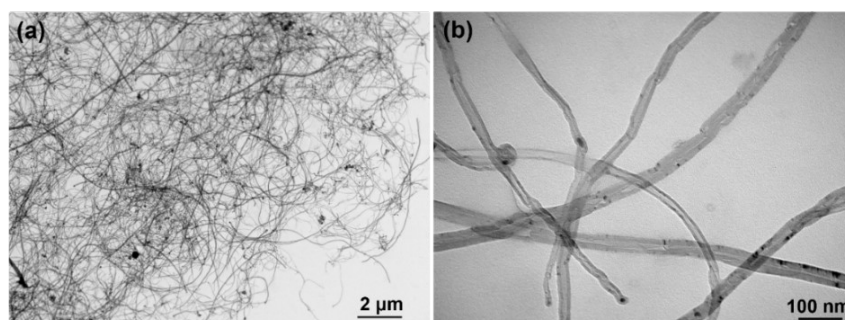

Fig. S3 TEM images of GONRs.
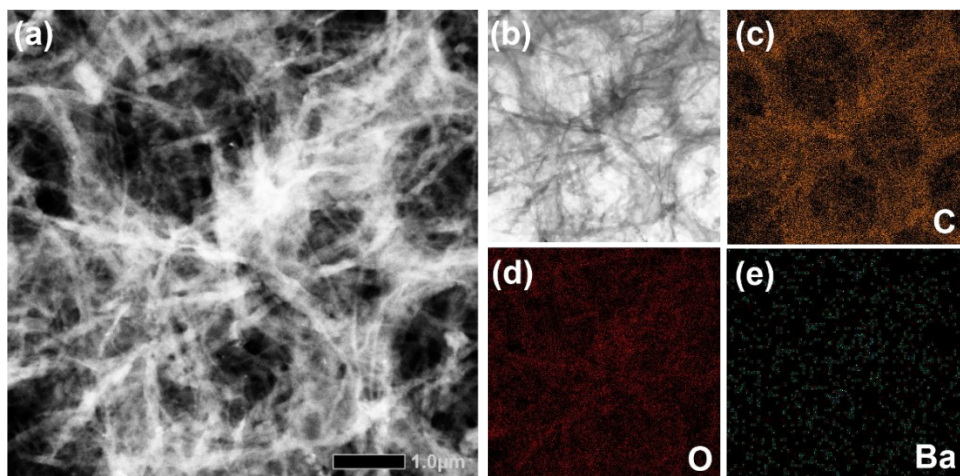

Fig. S4 TEM images of CNTs.

Fig. S5 (a) STEM image of the GONRs-Ba paper after strong ultrasonic treatment; (b) the corresponding TEM image of the GONRs-Ba paper; (c-e) the element mapping of the GONRs-Ba paper.
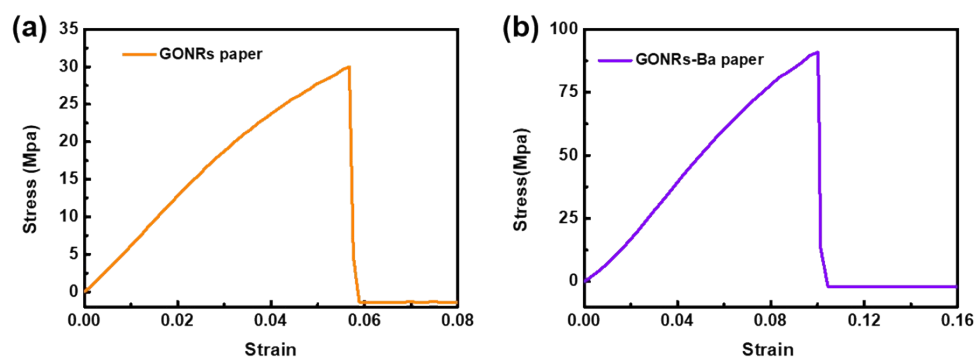

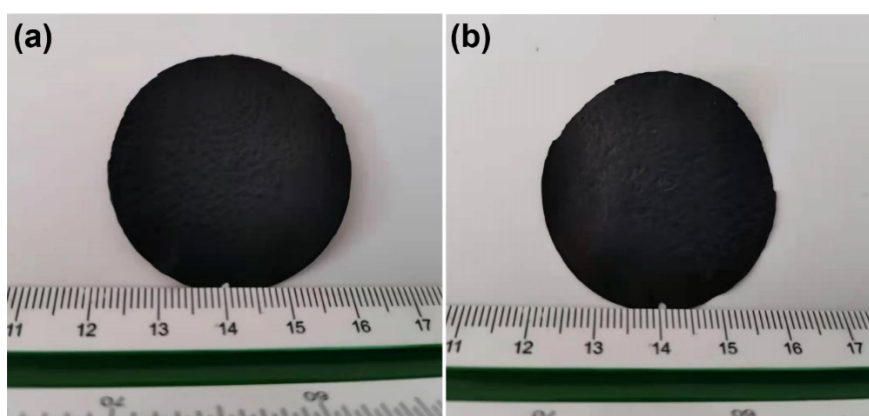**Fig. S6** Tensile stress/strain curves of (a) GONRs paper and (b) GONRs-Ba paper.

Fig. S7 Digital photographs of the GONRs-Ba paper in successive bending. (a) before bending; (b) after bending.
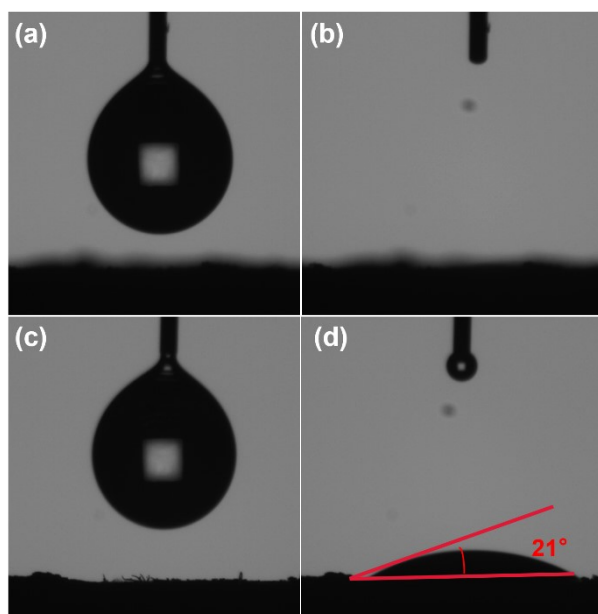
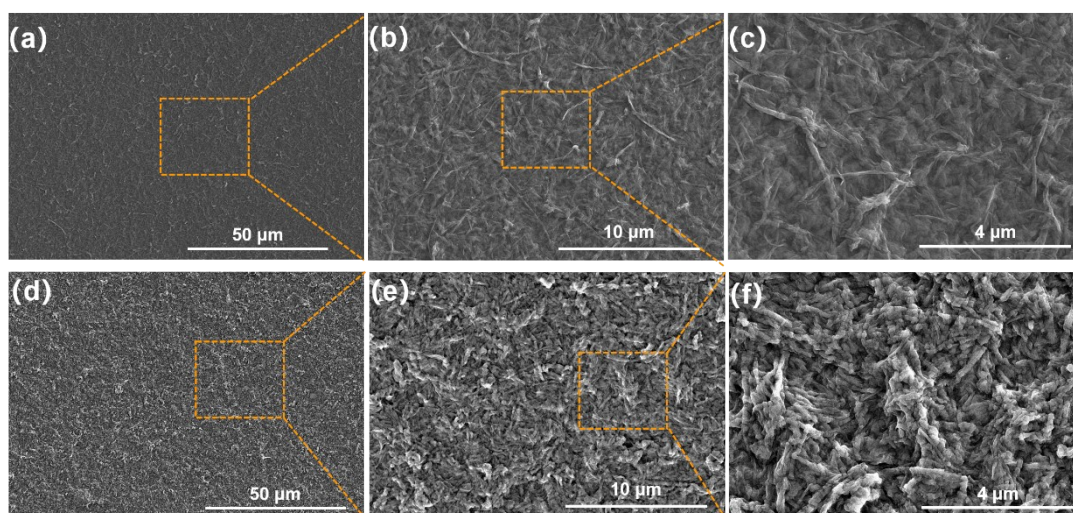**Fig. S8** Water contact angles of (a-b) GONRs paper and (c-d) GONRs-Ba paper.

Fig. S9 the FESEM images of GONRs paper (a-c) and GONRs-Ba paper (d-f).
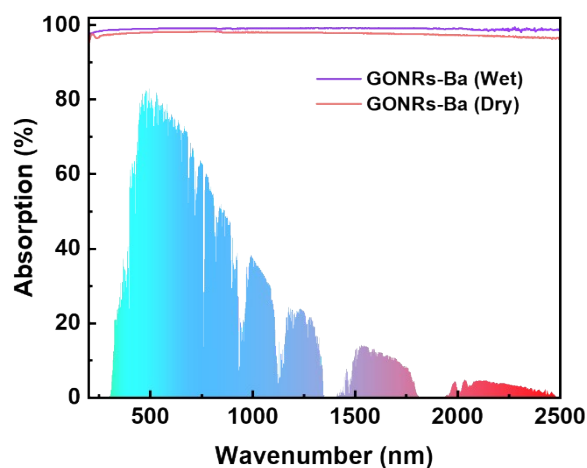
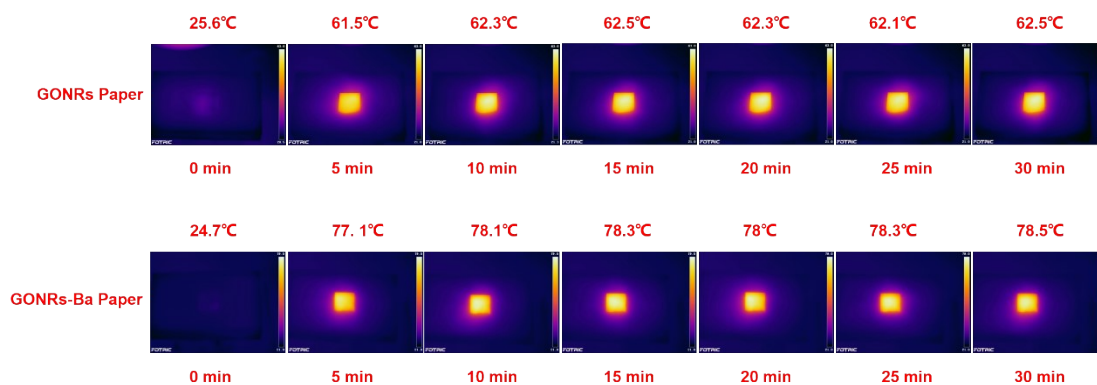**Fig. S10** Light absorption spectra for GONRs-Ba (Wet) and GONRs-Ba (Dry).

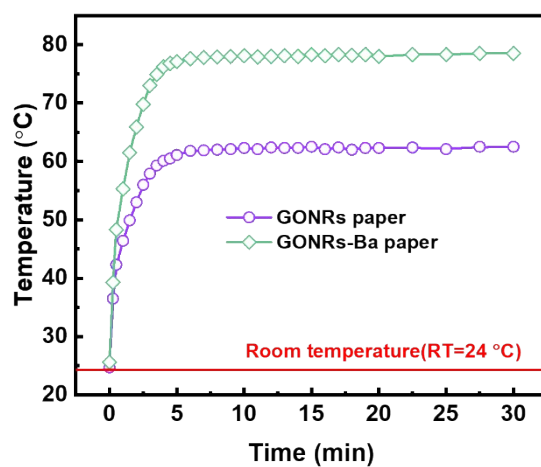**Fig. S11** IR thermal images of the samples without water under one solar intensity irradiation.

Fig. S12 Temperature changes over time of GONRs paper and GONRs-Ba paper without water under one solar intensity irradiation.
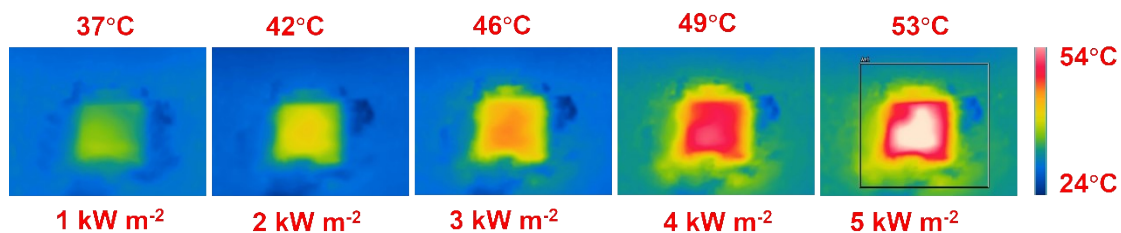
Fig. S13 IR thermal images of the GONRs-Ba paper without water under different solar intensity irradiation.
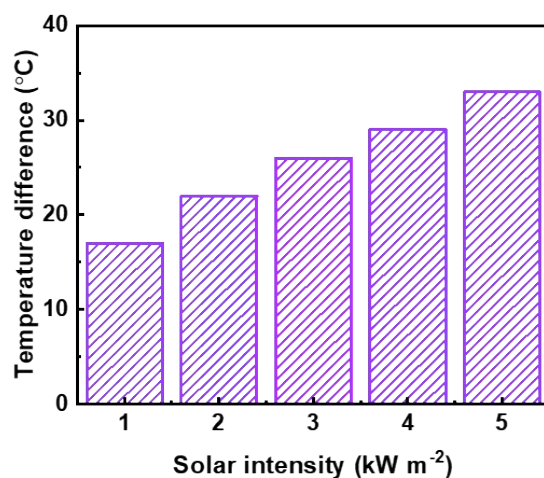

Fig. S14 Temperature differences of the GONRs-Ba paper with water under different solar intensities irradiation.
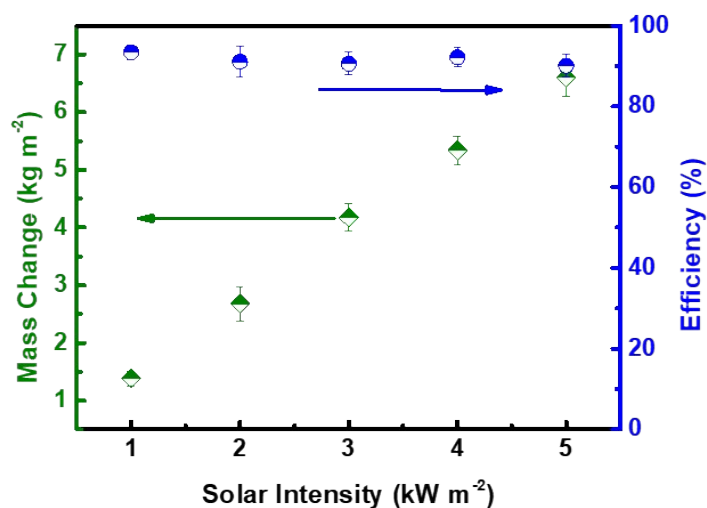
Fig. S15 Evaporation rates and evaporation efficiencies for evaporation devices based on GONRs-Ba paper under different solar intensities.

Fig. S16 Comparison of the evaporation rates of evaporator based on GONRs-Ba paper in different concentrations of brine under one solar intensity irradiation for 9 hours continuously.
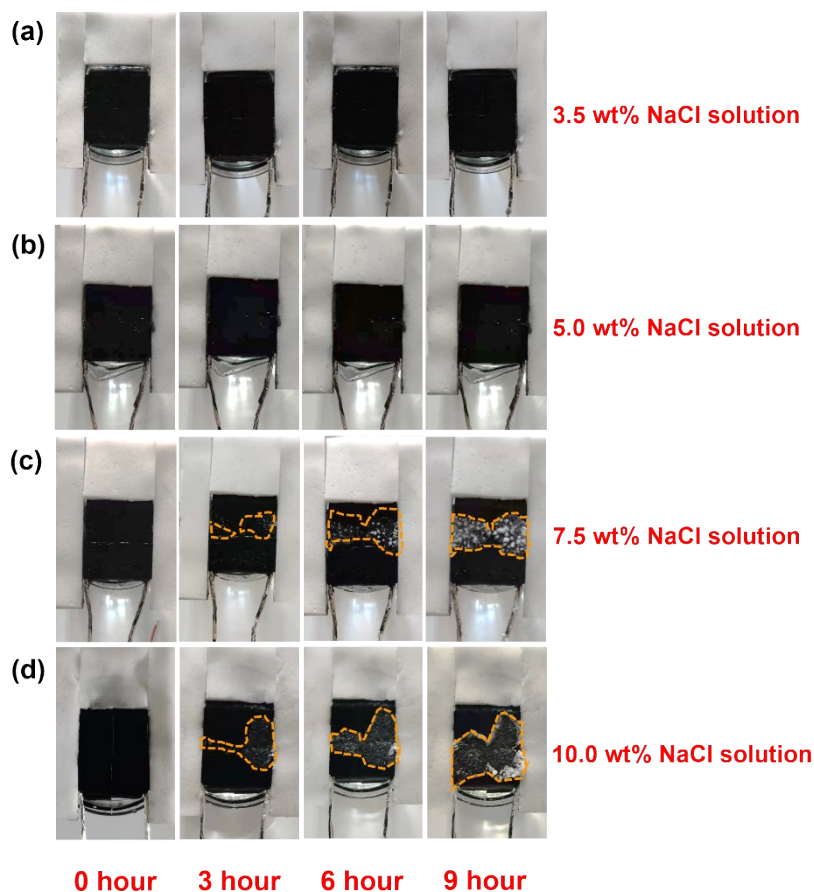
Fig. S17 The digital photographs of the evaporator based on GONRs-Ba paper with different concentration solutions of brine under continuous one intensity solar irradiation for 9 hours.

| 0 s | 4 s | 8 s | 12 s | 16 s |
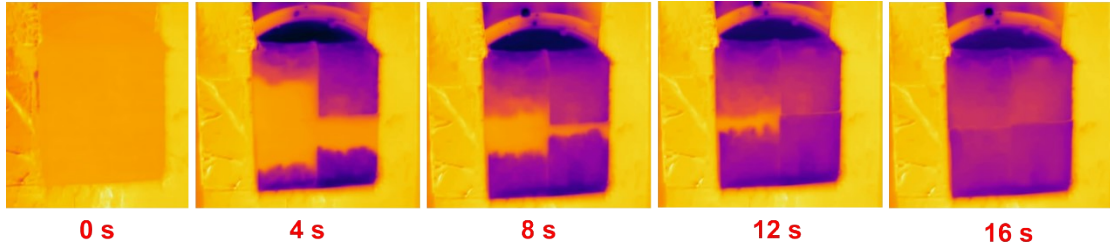
Fig. S18 The IR thermal photos of the water transport process.

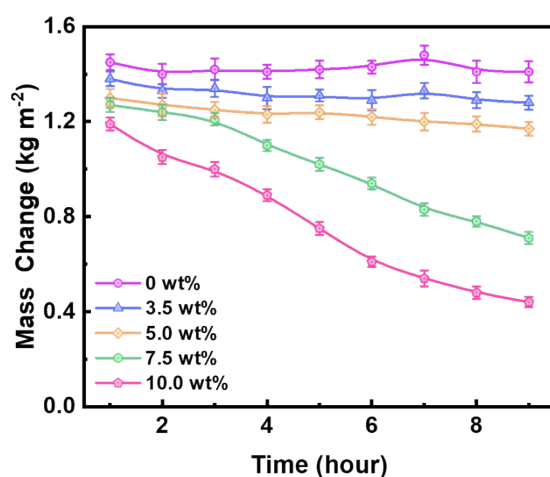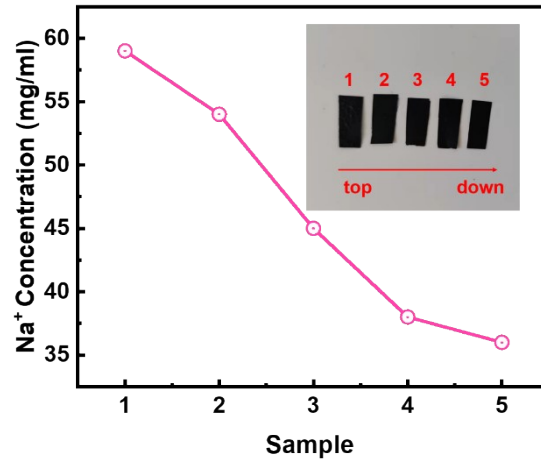**Fig. S19** The concentrations of Na$^+$ in different regions of the GONRs-Ba after 40 mins evaporated experiment.

Seawater　　　Deionized water　　　Condensed water

Fig. S20 Digital photographs for the resistance value comparison of seawater, deionized water and condensed water.
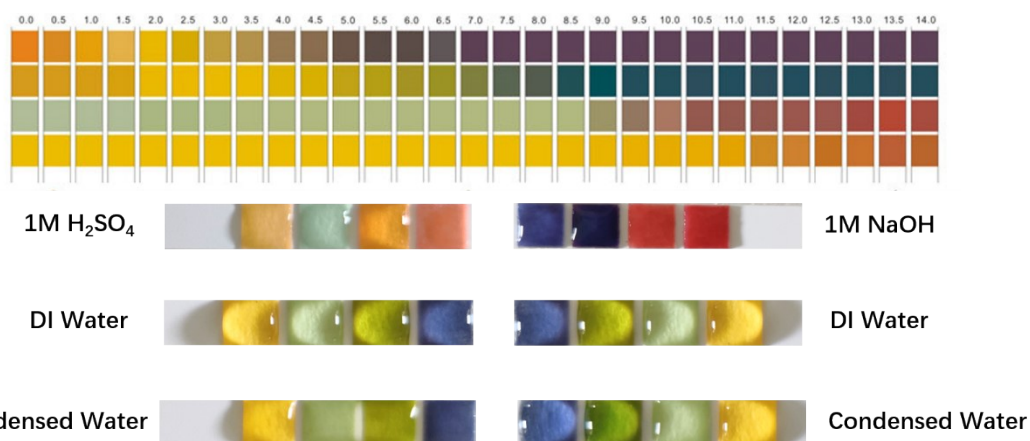
Fig. S21 Digital photos of pH test for acid and alkali solutions, deionized water and condensed water after GONRs-Ba paper evaporation under one solar intensity irradiation.
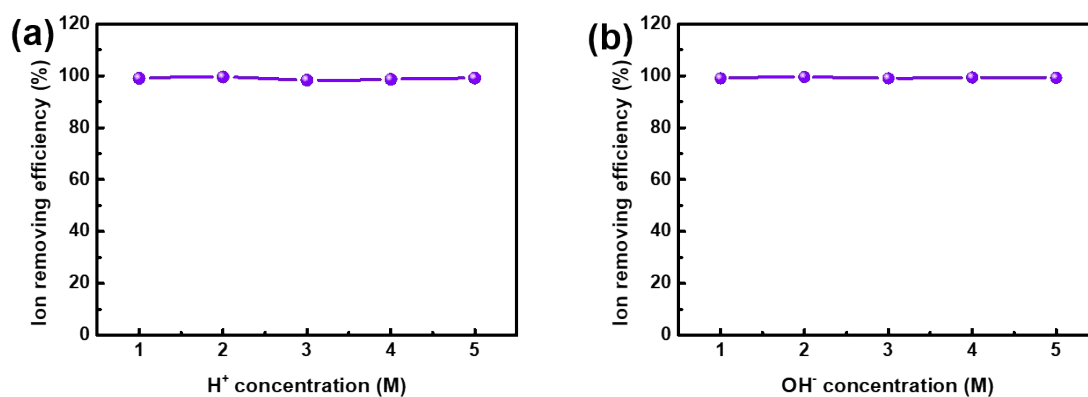
Fig. S22 Removing efficiencies for hydrogen ions and hydroxide ions over GONRs-Ba paper after solar thermal purification under one solar intensity irradiation.
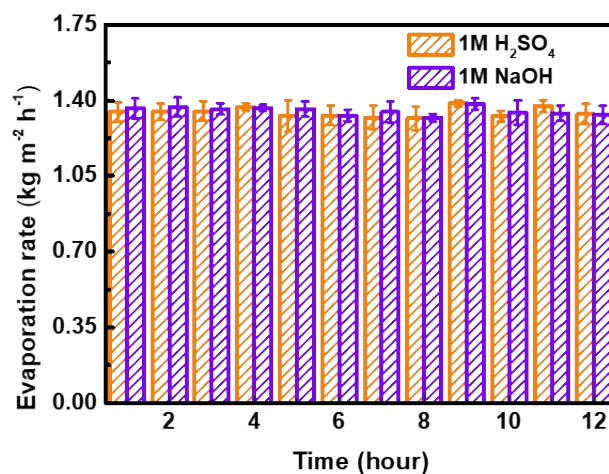
Fig. S23 Evaporation rates over GONRs-Ba paper under one solar illumination during

12 hours for strong acid and alkali solutions desalination under one solar intensity irradiation.

Fig. S24 Heavy metal ions rejecting efficiency over GONRs-Ba paper after solar thermal purification under one solar intensity irradiation.
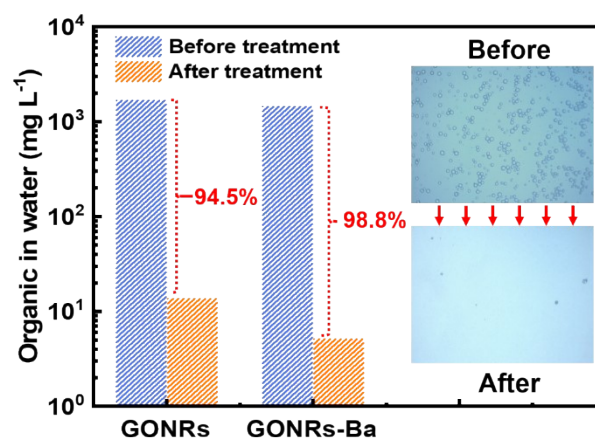
Fig. S25 Purification efficiency for emulsion utilizing the steam generator based on GONRs-Ba paper under one solar intensity irradiation. Inset, optical microscope images of pristine emulsion and the purified water from the emulsion.
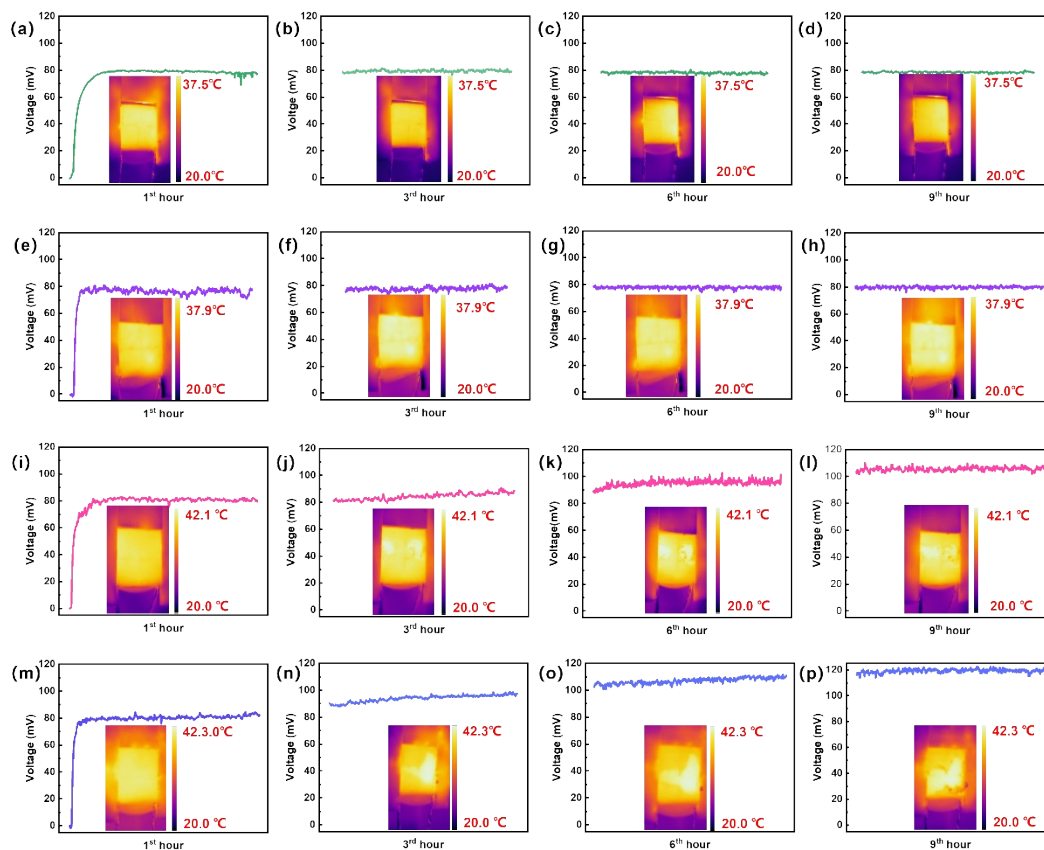
Fig. S26 The corresponding open-circuit voltages with different concentration solutions of brine in 1st, 3rd, 6th and 9th hour under one solar intensity irradiation. (a-d) 3.5 wt%; (e-h) 5.0 wt%; (i-l) 7.5 wt%;(m-p) 10.0 wt%. Inset: The corresponding IR thermal images with different concentration solutions of brine under continuous one intensity solar irradiation.
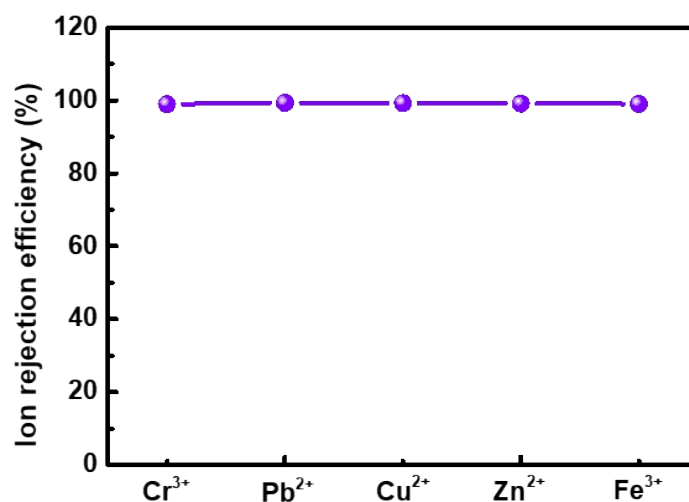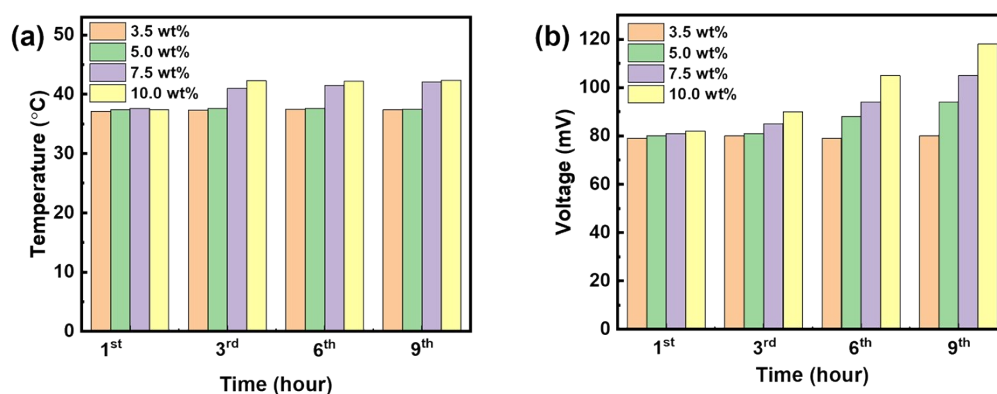

Fig. S27 The corresponding surface temperature and open-circuit voltage of evaporator based on GONRs-Ba paper with different concentration solutions of brine in 1st, 3rd, 6th, and 9th hour under one solar intensity irradiation.
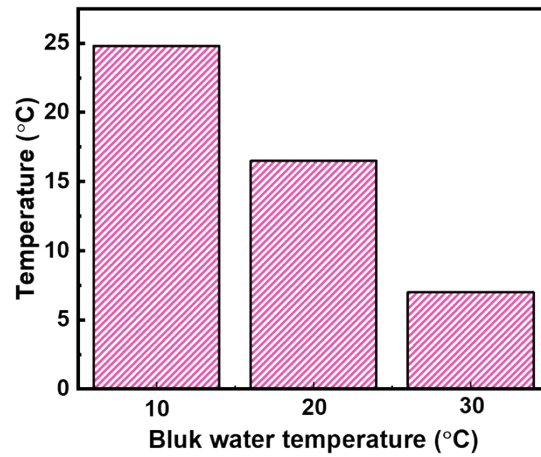
Fig. S28 Temperature difference between the evaporation device based on the GONRs-Ba paper and bulk water with different temperatures (10 °C, 20 °C, and 30 °C) under one solar intensity irradiation.
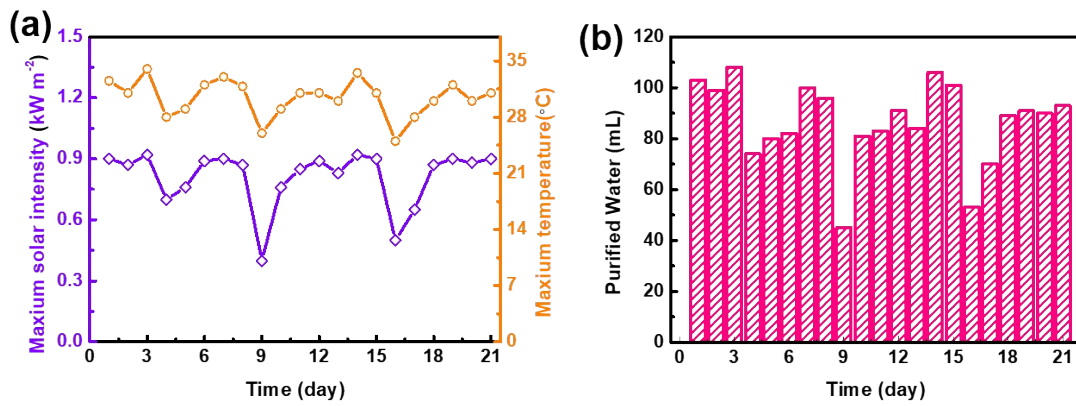
Fig. S29 Stability performance of the evaporation device based on GONRs-Ba paper outdoor. (a) The changes of ambient temperature and solar intensity under the sunlight within 21 days in August in Dalian, China. (b) The volume of collected water under the sunlight within 21 days.

Fig. S30 Stability performance of the output voltage for the evaporation device based on GONRs-Ba paper outdoor within 21 days in August in Dalian, China.

2. Supporting Notes

(a) Calculation of enthalpy of liquid-vapor phase transition on the Hess' Law in thermodynamics

In this work, the slope of the mass loss curve was utilized when the solar-driven interfacial steam devices remained in stable status, thus during which it could be considered that the water had been heated to the operating temperature. In the calculation of efficiency, it shou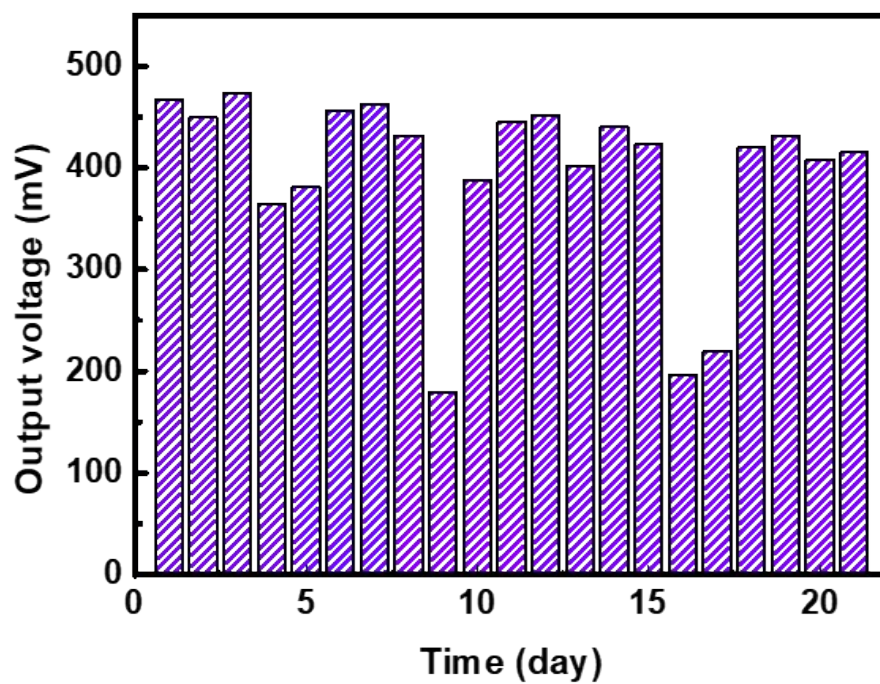ld be considered that water has different latent heat at different temperatures. To obtain an accurate latent heat at the specific temperature, a multistep equilibrium reaction route was constructed according to the Hess' Law：

$$\Delta H_{Ts} = \int_{T_s}^{100°C} C_{p,l} dT + \Delta H_{lv,100°C} + \int_{100°C}^{T_s} C_{p,v} dT$$

$$\text{Equation S1}$$

Among them, ΔH_{Ts} is the accurate latent heat of the water under different temperatures. $C_{p,l}$ is the heat capacity of liquid water, the value is about 4.183 J·K^{-1}·g^{-1} according to reference. $C_{p,v}$ is the heat capacity of water vapor, the value is about $(3.470 + 1.45×10^{-3} ×T + 0.121×105× T^{-2}) · R$ (J·K^{-1}·mol^{-1}), R= 8.314 J·K^{-1}·mol^{-1} according to references. $\Delta H_{lv,100°C}$ is the latent heat of the water under 100°C, the value is 2570 J·g^{-1} according to reference.

According to the above-mentioned formula, the accurate latent heat of the water under different temperatures is as followed form.

Table S1

Operating temperature of the absorbers (Ts, °C)	Latent heat (ΔH_{Ts}, J·g^{-1})
34.0	2410
34.5	2408
35.0	2407
35.5	2405
36.0	2404
36.5	2403
37.0	2402
37.5	2401
38.0	2400

(b) Heat loss characterization

1) Radiation loss:

The radiation loss was analyzed by Stefan-Boltzmann Equation.

$$E_R = \varepsilon A \delta\left(T_1^4 - T_2^4\right)$$
<div align="right">Equation S2</div>

E_R is heat flux (W), ε denotes emissivity (Supposing the evaporator has a maximum emissivity of 1), A is evaporation surface area (1 cm^{-2}), σ represents the Stefan-Boltzmann constant (σ= 5.670373×10^{-8} W m^{-2} K^{-4}), T_1 is the average surface temperature of the solar absorber after stable steam generation under one-sun illumination (37°C). T_2 is the ambient temperature around the evaporator (33°C). Therefore, based on Equation S2, we can calculate that the radiation heat loss is about 2.5%

2) Conduction loss:

The heat loss of convection was analyzed according to the following Equation.

$$Q = Cm\Delta T$$
<div align="right">Equation S3</div>

Q denotes the heat energy, C is the specific heat capacity of pure water (4.2 J °C^{-1} g^{-1}), m represents the weight of bulk water and ΔT is the increased temperature of the bulk water after stable steam generation. In our experimental, m = 5 g, ΔT = 0.2 °C for evaporation steam. Therefore, based on Equation S3, we can calculate that the conduction heat loss is ∼1%.

3) Convection loss:

The convection loss was calculated by Newton's law of cooling.

$$Q = hA\Delta T$$
<div align="right">Equation S4</div>

Q is the heat energy, h denotes the convection heat transfer coefficient (∼5 W m^{-2} K^{-1}) . A represents surface area. ΔT is difference between the ambient temperature around the evaporator and the surface temperature of the evaporator. Therefore, based on Equation S4, we can calculate that the convection heat loss of SG2 is ∼2%.

4) Reflection loss:

The solar absorption of solar absorber is 97 %; thus, the refection loss is ∼3 %.